Engineering Analysis with Boundary Elements 137 (2022) 78–90

Contents lists available at ScienceDirect

Engineering Analysis with Boundary Elements

journal homepage: www.elsevier.com/locate/enganabound

# The application of FEM-BEM coupling method for steady 2D heat transfer problems with multi-scale structure

Fei Qin [a,b], Qi He [a], Yanpeng Gong [a,b,*], Tong An [a,b], Pei Chen [a,b], Yanwei Dai [a,b]

[a] Institute of Electronics Packaging Technology and Reliability, Faculty of Materials and Manufacturing, Beijing University of Technology, Beijing, 100124, China
[b] Beijing Key Laboratory of Advanced Manufacturing Technology, Faculty of Materials and Manufacturing, Beijing University of Technology, Beijing, 100124, China

ARTICLE INFO

*Keywords:*
Boundary element method
Finite element method
Coupling method
ABAQUS
Heat transfer problem with multi-scale structures

ABSTRACT

This paper presents a finite element method and boundary element method (FEM-BEM) coupling scheme to study the steady-state 2D heat transfer problem for structures with multi-scale features. Based on the geometric information or material properties, the considered model is divided into FE sub-domain and BE sub-domain. The closed BE sub-domain in the mixed FEM-BEM model is defined as a finite super-element for which the effective stiffness matrix and effective fluxes are obtained by the self written BE code and hence can be assembled to the FE systems by the user subroutine (UEL) provided in ABAQUS. This method offers a number of key improvements compared with current analysis methods available for multi-scale structures. These improvements are: (i) the flexibility and convenience by using the powerful pre/post-processing in ABAQUS; (ii) the higher accuracy of the solution over the classical FEM; and (iii) the computational cost and time can be highly reduced by using the coupling method. Numerical results are compared with reference solutions and demonstrate the accuracy and effectiveness of the proposed approach.

## 1. Introduction

With increasing requirements of high performance and small size electronic equipments, power densities of semiconductor devices are continuously rising, which results in high heat flux in electronic equipments. In recent years, the use of electronic devices in various industries has given a more careful attention to this section [1]. One of the main issues discussed in relation to the electronic devices is the analysis of heat transfer problems, which is essential to perform the thermal management/design of electronic devices for researchers and engineers. Since the characteristics of simple implementation and low cost, numerical methods are becoming a widely used way to provide guidances for the design of electronic devices. Up to now, many numerical methods have been developed to study the heat transfer problems, such as finite element method (FEM) [2], mesh free method (MFM) [3], finite difference method (FDM) [4], boundary element method (BEM) [5], traction boundary elements method (TBEM) [6], method of fundamental solutions (MFS) [7], etc. Many of the numerical schemes can be used to study the heat transfer problems in electronic equipments [8–11].

In [12], Yun et al. presented an RC component model (RCCM) to extract thermal resistances and time constants for a thermal network. The method enables a system designer to couple the thermal prediction with a circuit simulator to analyze the electrothermal behavior of insulated gate bipolar transistor (IGBT) module system, simultaneously. To optimize the heat conduction in Fan-out (FO) package, Huang et al. proposed a hybrid method using Taguchi design of experiments, radial basis neural network (RBNN) and genetic algorithm (GA) in [13]. To help electronic designers find the optimum placement of some heating devices, some guidelines based on analytical approach model is proposed in [14]. Actually, due to the emergence of FEM professional softwares (ANSYS, ABAQUS, COMSOL, etc.), the FEM is becoming the most popular numerical method for the heat transfer of the electronic device. In [15], Oda and Sakamoto presented a special finite-element method which provides attractive results without three-dimensional finite-element discretization to study the multiple laminated structure in electronic packaging. In [16], the COMSOL Multiphysics is adopted to build the multi-chips module combined with ball grid array (MCM-BGA) 3D package model, which allows running a coupled thermo-fluidic FEM simulation. Based on the simulation, the multi-parameters optimization of structural parameters was conducted. To investigate the thermal response of sample boards (at board level) during the preheating stage of the reflow process, a forced-convection reflow oven was modeled using computational fluid dynamic software FLUENT, whereas structural heating at the board level was conducted using finite-element method software ABAQUS [17].

* Corresponding author.
*E-mail address:* yanpeng.gong@bjut.edu.cn (Y. Gong).

https://doi.org/10.1016/j.enganabound.2022.01.009
Received 12 September 2021; Received in revised form 27 December 2021; Accepted 13 January 2022
Available online 2 February 2022

It should be noted that models with multi-scale structures are highly challenging because small and large features of structures occur in one model, which requires discretization of the computational domain, resulting in very large degrees of freedom. Although many approaches have been presented to study electronic devices, there are few approaches to analyze heat transfer problems of the electronic module systems with multi-scale structures. This is due to the limitations of computational time and the available computer memory for fine meshes. For a numerical model with coatings or thin sections, the size of each element should be close to the thickness of the coatings or thin sections, which may result in too many elements in discretizing the model [18,19]. Since the advantages of reduction dimensionality of the problem by one and the high accuracy of its solutions on boundary element meshes, the boundary element method (BEM) seems to be a great alternative for the analysis of semiconductor structures.

In [20], Khatir and Lefebvre investigate thermal behavior of high power semiconductor packages subjected to power cycling loads by using the boundary element method. Based on boundary element method, Vermeersch and Mey studied dynamic thermal characterization of electronic packages [21]. The authors found that the results obtained by BEM agree well with analytical results. And the method could easily be extended to multi-layer structures and more complicated package configurations. In [22], an analysis method based on the boundary element method is presented to study the transient thermal response of electronic packages consisting of dissimilar materials while subjected to general boundary conditions. To carry out stress calculation of the integrated circuit (IC) plastic package under the remote loading or the pressure acting on the delamination surfaces, Dong and Lee presented a boundary element method in which fundamental solutions derived from the symmetrical property of studied problem are adopted [23]. More recently, Yu et al. presented an isogeometric boundary element method (IGABEM) to study the heat transfer problems of electronic packaging structure [24]. It should be noted that there are also some limitations in the application of BEM for some electronic package problems. For the analysis of multi-scale structures, large number of nearly singular integral which presents challenges for practitioners working with the BEM appears. Due to the coefficient matrices of BEM are dense and nonsymmetrical, the computation time of forming and solving the systems for a whole complicated model is enormous. In addition, the fundamental solution (needed in BEM analysis) of some materials is difficult to obtain, especially for 3D problems [25].

In 2010, Tadeu et al. proposed a BEM/TBEM and MFS coupling method for the transient analysis of conduction heat transfer in the presence of inclusions and layers structures with thicknesses nearly zero [26]. From the results we can find that the coupling scheme overcomes the limitations posed by each method. Inspired by this work, the coupling of FEM and BEM seems to be a good way for the analysis of the semiconductor devices with large number of multi-scale structures. The coupling method combines the advantages of BEM and FEM while not requiring any iterations along the interfaces between BEM and FEM domains. This type of coupled formulation avoids the fine discretization required by FEM to achieve accurate results in regions with small length scales and geometric and material discontinuities [27]. The FEM–BEM coupling scheme has been studied for a long time. In 1977, Zienkiewicz and Bettess proposed the scheme how the BEM can be utilized in conventional FEM context [28].

Then, the coupling scheme is widely used in several fields, including elasticity problems [29,30], potential problems [31], heat transfer problems [32], geomechanics [33], electronic packages problems [22], magnetic field problems [34–36], acoustic problems [37], contact problems [38]. The coupling scheme of isogeometric analysis (IGA) and isogeometric boundary element method (IGABEM) have been investigated by many researchers in recent years [39,40]. Some literature survey on the coupling of BEM and FEM can be found in [41,42]. In 2016, Liu and Dong presented an automatic implementation procedure for the coupling of the ABAQUS with a BEM code to study dynamic elastoplastic problems [43]. By using this coupling scheme, the user can not only benefit from the powerful pre- and post-disposal functions of the ABAQUS, but also deal with infinite problems by adopting the BEM as a supplement. Based on the powerful platform of the ABAQUS, the coupling scheme will be a potential method for the thermal analysis of electronic packaging structure.

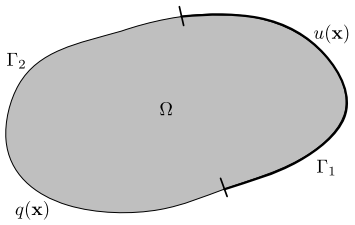


**Fig. 1.** Model subjected to heat transfer.

In this paper, based on the commercial finite element analysis software ABAQUS, we propose a coupling method of FEM-BEM and apply this scheme to study the steady-state heat transfer problem. For a numerical model with multi-scale features (large part and small part existing in one model), to reduce the number of element used in the computation, we divide the model into different parts. To avoid the evaluation of nearly singular integrals in BEM, the small part is studied by FEM and large part is analyzed by BEM. For a model with different materials, the BEM will be used in the domain with linear elastic materials, while FEM is used to analyze the other domain with complex materials properties. In the numerical implementation of the coupling scheme, based on the geometric features or material property of the computed model, the model should be divided into two sections: the BE part and FE part. The boundary element method will be used in the BE part, and finite element method is used in the FE part. The interface (line element for 2D problems and surface element for 3D problems) between the FE part and BE part is regarded as a super-element which can be incorporated into the finite element code. A self-written BEM code for heat transfer problems is developed to realize the coupling scheme. The BEM code will be started inside UEL to calculate the effective stiffness and effective fluxes on the interface of BE part and FE part, the relationship of which are handled as the given boundary conditions for the FE part. Then the global coupling stiffness matrix which is consisted of the stiffness matrix of BEM and the stiffness matrix of FEM can be obtained. The resulted system equations is solved by the solver of ABAQUS. In this work, the user subroutine URDFIL is used to pass the relative information to the BE code for the BE part analysis.

The outline of this paper is shown as follows. Some formulations of the FEM and BEM for heat transfer problem is briefly introduced in Section 2. Section 3 presents the implementation of the coupling scheme for heat transfer problems. In Section 4, the process of coupling ABAQUS and the BEM code is presented. Some numerical examples for plate and BGA are analyzed in Section 5 to demonstrate the correctness and efficiency of the coupled method. Finally, some discuss and conclusions are given in Section 6.

## 2. Theoretical analysis

In this section, we will outline the fundamentals of the finite element method and boundary element method for 2D steady-state heat transfer problems in isotropic medium. For these problems, the structure occupies a continuous physical domain, $\Omega \in R^2$ with closed boundary $\Gamma$, as shown in Fig. 1. It is assumed for simplicity in this paper that the domain is free of thermal sources/sinks in the heat transfer problem. The governing equations for isotropic materials are [44]

$$\nabla^2 u(\mathbf{x}) = \frac{\partial}{\partial x_i}\left(k\frac{\partial u(\mathbf{x})}{\partial x_i}\right) = 0, \tag{1}$$

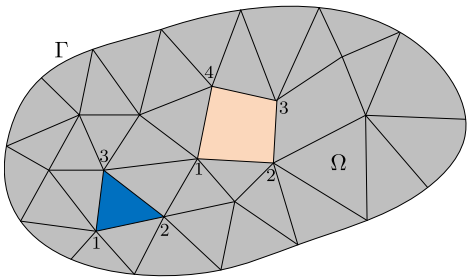


**Fig. 2.** Discretization of the model for FEM.

where $\nabla^2$ is the Laplace operator; $\mathbf{x}$ represents coordinate vector; $k$ denotes the thermal conductivity; the summation rule is applied to the index $i = 1, 2$ for 2D problems and $u(\mathbf{x})$ is the temperature function at point $\mathbf{x}(x_1, x_2) \in \Omega$.

For heat transfer problems, the heat flux density in direction $x_i$ can be obtained by

$$q_i = k\frac{\partial u(\mathbf{x})}{\partial x_i} \tag{2}$$

where $i = 1, 2$ for 2D problems. And for points at boundary curve or surface $\Gamma$, the normal flux density $q$ is used and defined as

$$q = -k\frac{\partial u(\mathbf{x})}{\partial \mathbf{n}} \tag{3}$$

where $\mathbf{n}$ is the outward pointing normal.

Eq. (1) can be solved subjected to a set of boundary conditions taken from the following

$$u(\mathbf{x}) = \bar{u}(\mathbf{x}), \quad \mathbf{x} \in \Gamma_1, \tag{4}$$

$$q(\mathbf{x}) = \bar{q}(\mathbf{x}), \quad \mathbf{x} \in \Gamma_2, \tag{5}$$

where $\bar{u}$ and $\bar{q}$ are known temperature and flux densities, respectively. $\Gamma_1$ and $\Gamma_2$ denote the Dirichlet and Neumann boundaries, with $\Gamma = \Gamma_1 \cup \Gamma_2$ and $\Gamma_1 \cap \Gamma_2 = \emptyset$.

### 2.1. Finite element formulations for the steady-state heat transfer problem

Consider a two-dimensional body in heat transfer conditions as shown in Fig. 1, and consider steady-state conditions. For the heat transfer analysis we assume that the material obeys the Fourier's law of heat conduction. The FEM system equations of this problem can be formulated by the weighted residual approach [45].

Firstly, the governing equation in Eq. (1) can be expressed as [46]

$$f(u(\mathbf{x})) = k\left(\frac{\partial^2 u}{\partial x_1^2} + \frac{\partial^2 u}{\partial x_2^2}\right) = 0, \tag{6}$$

where $\mathbf{x} = (x_1, x_2)$ and $f$ is a function defined by

$$f(u(\mathbf{x})) = k\left(\frac{\partial^2 u}{\partial x_1^2} + \frac{\partial^2 u}{\partial x_2^2}\right).$$

Based on the idea of weighted residual approach, a good approximation to the exact solution of $u(\mathbf{x})$, which satisfies Eq. (6) can be obtained by solving the following weighted integral equation

$$\int_A W f(u(x_1, x_2))dx_1 dx_2 = 0, \tag{7}$$

where $W$ is the weight function and $A$ denotes the computed domain.

To improve the accuracy of the approximation, the computed domain can be divided into smaller sub-domains (elements) as shown in Fig. 2.

For each element, it is assumed that

$$u^h(x_1, x_2) = \mathbf{N}(x_1, x_2)\mathbf{u}^e \tag{8}$$

where $u^h$ is the approximated temperature and $\mathbf{u}^e$ is the temperature at the nodes of the element, and

$$\mathbf{N} = [N_1, N_2, \ldots, N_{n_d}], \tag{9}$$

where $N_i$ is the shape function of $(x_1, x_2)$, and $n_d$ is the number of the nodes of each element ($n_d = 3$ for triangular element and $n_d = 4$ for quadrilateral element).

For the Galerkin method, the shape functions are usually used as the weight function. Based on the Galerkin method, the residual ($\mathbf{R}^e$) calculated at all the nodes for an element is then evaluated by the following equation [2]

$$\mathbf{R}^{(e)} = \int_{A_e} \mathbf{N}^T f(u(x_1, x_2))dA_e \tag{10}$$

where $A_e$ is the area of the element.

To obtain the element matrices, the integral in the Eq. (10) must be evaluated. Based on Eq. (6), Eq. (10) can be written as

$$\mathrm{R}^{(e)} = \int_{A_e} \mathbf{N}^T k(\frac{\partial^2 u}{\partial x_1^2} + \frac{\partial^2 u}{\partial x_2^2})dA_e \tag{11}$$

By using the product rule for differentiation, we can obtain

$$\frac{\partial}{\partial x_1}(\mathbf{N}^T\frac{\partial u}{\partial x_1}) = \mathbf{N}^T\frac{\partial^2 u}{\partial {x_1}^2} + \frac{\partial \mathbf{N}^T}{\partial x_1}\frac{\partial u}{\partial x_1} \tag{12}$$

Then, the first part of Eq. (11) can be written as

$$\int_{A_e} \mathbf{N}^T k\frac{\partial^2 u}{\partial x_1^2}dA_e = \int_{A_e} k\frac{\partial}{\partial x_1}(\mathbf{N}^T\frac{\partial u}{\partial x_1})dA_e - \int_{A_e} k\frac{\partial \mathbf{N}^T}{\partial x_1}\frac{\partial u}{\partial x_1}dA_e \tag{13}$$

According to the Gauss's divergence theorem, the first integral of the right side of Eq. (13) can be expressed as:

$$\int_{A_e} k\frac{\partial}{\partial x_1}(\mathrm{N}^T\frac{\partial u}{\partial x_1})dA_e = \int_{\Gamma_e} \mathrm{N}^T\frac{\partial u}{\partial x_1}\cos\theta d\Gamma \tag{14}$$

where $\theta$ is the angle of the outwards normal $\mathbf{n}$ on the boundary $\Gamma_e$ of the element with respect to the $x$ axis. Substituting Eq. (14) into Eq. (13) yields the following equation:

$$\int_{A_e} \mathrm{N}^T k\frac{\partial^2 u}{\partial x_1^2}dA_e = \int_{\Gamma_e} \mathrm{N}^T k\frac{\partial u}{\partial x_1}\cos\theta d\Gamma - \int_{A_e} k\frac{\partial \mathrm{N}^T}{\partial x_1}\frac{\partial u}{\partial x_1}dA_e \tag{15}$$

Similarly, the following equation can be obtained

$$\int_{A_e} \mathrm{N}^T k\frac{\partial^2 u}{\partial x_2^2}dA_e = \int_{\Gamma_e} \mathrm{N}^T k\frac{\partial u}{\partial x_2}\sin\theta d\Gamma - \int_{A_e} k\frac{\partial \mathrm{N}^T}{\partial x_2}\frac{\partial u}{\partial x_2}dA_e \tag{16}$$

From Eqs. (15) and (16) we obtain:

$$\begin{aligned}\mathrm{R}^{(e)} = &\left[\int_{A^e} k\left(\frac{\partial \mathrm{N}^T}{\partial x_1}\frac{\partial \mathrm{N}}{\partial x_1} + \frac{\partial \mathrm{N}^T}{\partial x_2}\frac{\partial \mathrm{N}}{\partial x_2}\right)dA\right]u^{(e)} \\ &- \int_{\Gamma_e} \mathrm{N}^T k\left(\frac{\partial u}{\partial x_1}\cos\theta + \frac{\partial u}{\partial x_2}\sin\theta\right)d\Gamma\end{aligned} \tag{17}$$

Then, the following matrix form can be obtained

$$\mathbf{R}^{(e)} = \mathbf{k}_D^{(e)}\mathbf{u}^{(e)} - \mathbf{b}^{(e)} \tag{18}$$

where

$$\mathbf{b}^{(e)} = \int_{\Gamma_e} \mathbf{N}^T k\left(\frac{\partial u^h}{\partial x_1}\cos\theta + \frac{\partial u^h}{\partial x_2}\sin\theta\right)d\Gamma, \tag{19}$$

$$\mathbf{k}_D^{(e)} = \int_{A_e} k\left(\frac{\partial \mathbf{N}^T}{\partial x_1}\frac{\partial \mathbf{N}}{\partial x_1} + \frac{\partial \mathbf{N}^T}{\partial x_2}\frac{\partial \mathbf{N}}{\partial x_2}\right)dA, \tag{20}$$

were $\mathbf{b}^{(e)}$ is a vector related to the derivatives of temperature (heat flux) on the boundaries of the element $\Gamma_e$.

Assume the gradient vector of temperature $\nabla\mathbf{u}$ as

$$\nabla\mathbf{u} = \begin{Bmatrix}\frac{\partial u}{\partial x_1}\\ \frac{\partial u}{\partial x_2}\end{Bmatrix} = \begin{Bmatrix}\frac{\partial N}{\partial x_1}\\ \frac{\partial N}{\partial x_2}\end{Bmatrix}\mathbf{u}^{(e)} = \mathbf{B}\mathbf{u}^{(e)} \tag{21}$$

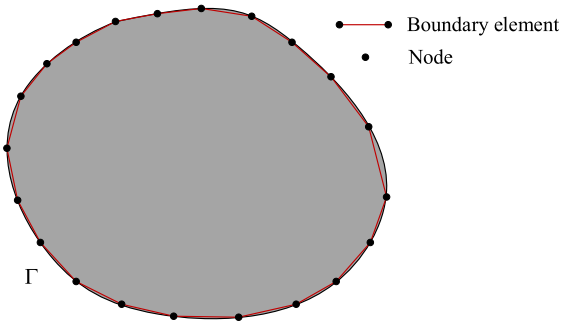


**Fig. 3.** Discretization of the model for BEM.

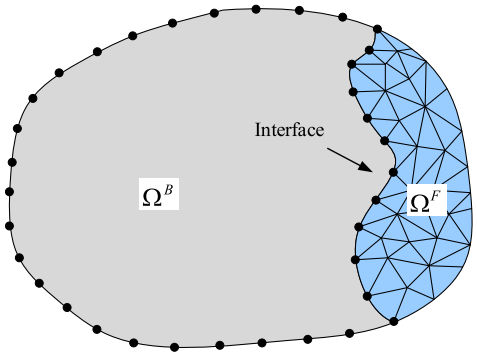


**Fig. 4.** A model divided into two sub-domains.

where **B** is given by

$$\mathbf{B} = \begin{bmatrix} \frac{\partial \mathbf{N}}{\partial x_1} \\ \frac{\partial \mathbf{N}}{\partial x_2} \end{bmatrix} = \begin{bmatrix} \frac{\partial N_1}{\partial x_1} & \frac{\partial N_2}{\partial x_1} & \cdots & \frac{\partial N_{n_d}}{\partial x_1} \\ \frac{\partial N_1}{\partial x_2} & \frac{\partial N_2}{\partial x_2} & \cdots & \frac{\partial N_{n_d}}{\partial x_2} \end{bmatrix} \tag{22}$$

where $n_d$ is the number of the nodes of each element.

Then the element stiffness matrix $\mathbf{k}_D^{(e)}$ for the 2D elements can be written as

$$\mathbf{k}_D^{(e)} = \int_{A_e} k\mathbf{B}^T\mathbf{B}dA \tag{23}$$

After obtaining the element matrices, the residual in Eq. (18) is assembled and enforced to equal to zero. And the global system of equations for FEM will be established as

$$[\mathbf{K}]\{\mathbf{u}\} = \{\mathbf{F}\} \tag{24}$$

where matrix $[\mathbf{K}]$ and $\{\mathbf{F}\}$ are assembled by the $\mathbf{k}_D^{(e)}$ and $\mathbf{b}^{(e)}$.

### 2.2. Boundary element formulations for the steady-state heat transfer problem

For a 2D heat transfer problem, the corresponding boundary integral equation (BIE) can be written as [47]

$$cu(\mathbf{y}) = \int_\Gamma t(\mathbf{x})U(\mathbf{y},\mathbf{x})d\Gamma(\mathbf{x}) - \int_\Gamma u(\mathbf{x})T(\mathbf{y},\mathbf{x})d\Gamma(\mathbf{x}) \tag{25}$$

where $\mathbf{y}$ and $\mathbf{x}$ are the source point and field point, respectively. $c = 0.5$ for smooth boundary points; $u(\mathbf{x})$ and $q(\mathbf{x})$ represent the temperature and the normal derivative (the heat flux) at point $x$ on boundary $\Gamma$. $U(\mathbf{y},\mathbf{x})$ and $T(\mathbf{y},\mathbf{x})$ denote the temperature and flux fundamental solution kernels, which are defined by

$$U(\mathbf{y},\mathbf{x}) = \frac{1}{2\pi k}\ln\left(\frac{1}{r}\right) \tag{26}$$

and

$$T(\mathbf{y},\mathbf{x}) = -k\frac{\partial U}{\partial r}\frac{\partial r}{\partial \mathbf{n}} \tag{27}$$

where $r$ is the Euclidean distance between source point $\mathbf{y}$ and field point $\mathbf{x}$.

To obtain the numerical solution of the boundary integral equation in Eq. (25), the boundary $\Gamma$ should be considered to be divided into boundary elements $\Gamma_e$ as show in Fig. 3. And the temperature and flux density fields around the boundary are expressed using the following interpolation functions:

$$u(\xi) = \sum N_n(\xi)u_n^e \tag{28}$$

$$t(\xi) = \sum N_n(\xi)t_n^e \tag{29}$$

where $\xi$ is the local coordinate; $N_n(\xi)$ is the interpolation functions; the superscript $e$ represents element index and the subscript $n$ represents the $n$th node of element $\Gamma_e$.

Replacing the continuous functions $u$ and $t$ in (25) by the expansions (28) and (29), the boundary integral equation in Eq. (25) is written in a discretized form

$$\begin{aligned} cu(\xi_i^p) = &\sum_{e=1}^{E}\sum_{n=1}^{N_e} t_n^e \int_{\Gamma_e} N_n(\xi)U(\xi_i^p,\xi)d\Gamma(\xi) \\ &- \sum_{e=1}^{E}\sum_{n=1}^{N_e} u_n^e \int_{\Gamma_e} N_n(\xi)T(\xi_i^p,\xi)d\Gamma(\xi) \end{aligned} \tag{30}$$

where $\xi_i^p$ is the local coordinate of the $i$th node point; $E$ denotes the total number of boundary elements and $N_e$ represents the number of nodes for each element. The Eq. (30) can be further simplified as:

$$cu(\xi_i^p) + \sum_{e=1}^{E}\sum_{n=1}^{N_e} u_n^e \Delta T_{ni}^e = \sum_{e=1}^{E}\sum_{n=1}^{N_e} t_n^e \Delta U_{ni}^e \tag{31}$$

Here,

$$\Delta U_{ni}^e = \int_{\Gamma_e} N_n(\xi)U(\xi_i^p,\xi)d\Gamma(\xi) \tag{32}$$

$$\Delta T_{ni}^e = \int_{\Gamma_e} N_n(\xi)T(\xi_i^p,\xi)d\Gamma(\xi). \tag{33}$$

If the boundary integral equation is applied for all the nodes, Eq. (31) can form the matrix as follows

$$[H]\{u\} = [G]\{t\} \tag{34}$$

where $\{u\}$ and $\{t\}$ represent the vectors contained temperature and fluxes at boundary nodes. $[H]$ is the coefficient matrix assembled by the solution kernel $T$ and coefficient $c$. $[G]$ is a rectangular matrix of solution kernel $U$.

Applying boundary conditions to Eq. (34), a linear system equations will be obtained as follows:

$$\mathbf{Ax} = \mathbf{b} \tag{35}$$

where matrix **A** contains the integral values related to the unknown temperature and heat flux, vector **x** includes the unknown temperature and heat flux, and **b** is a column vector composed of known quantities.

## 3. Coupled method of FEM-BEM

In this section, a FEM–BEM coupling scheme, which is efficient for solving multi-scale problems will be introduced. As shown in Fig. 4, the model is divided into two parts ($\Omega^B$ and $\Omega^F$). Here, the domain $\Omega^B$ represents that the boundary element method is used in the region. And domain $\Omega^F$ means the finite element method will be adopted to analyze this region. The mesh of the model used in the coupling scheme is also given in Fig. 4. Here, some detailed information of the coupling scheme will be given.

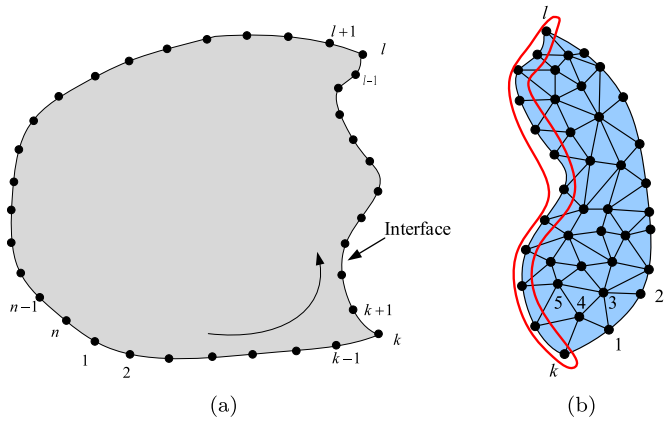


**Fig. 5.** Nodal locations of the two sub-domains: (a) Nodes for BEM (the interface nodal index is from $k$ to $l$), (b) Nodes for FEM (the interface nodal index is also from $k$ to $l$ in the red curve).

### 3.1. Formulations of FEM domain

According to the nodal locations shown in Fig. 5(b), the system equation in Eq. (24) can be expressed as

$$\begin{bmatrix} K_1^1 & \cdots & K_1^{k-1} & K_1^k & \cdots & K_1^l & K_1^{l+1} & \cdots & K_1^n \\ K_2^1 & \cdots & K_2^{k-1} & K_2^k & \cdots & K_2^l & K_1^{l+1} & \cdots & K_2^n \\ \vdots & \ddots & \vdots & \vdots & \ddots & \vdots & \vdots & \ddots & \vdots \\ K_{n-1}^1 & \cdots & K_{n-1}^{k-1} & K_{n-1}^k & \cdots & K_{n-1}^l & K_1^{l+1} & \cdots & K_{n-1}^n \\ K_n^1 & \cdots & K_n^{k-1} & K_n^k & \cdots & K_n^l & K_1^{l+1} & \cdots & K_n^n \end{bmatrix} \times \begin{Bmatrix} u_1 \\ \vdots \\ u_{k-1} \\ u_k \\ \vdots \\ u_l \\ u_{l+1} \\ \vdots \\ u_n \end{Bmatrix} = \begin{Bmatrix} F_1 \\ \vdots \\ F_{k-1} \\ F_k \\ \vdots \\ F_l \\ F_{l+1} \\ \vdots \\ F_n \end{Bmatrix} \tag{36}$$

To be able to use the coupling scheme, the above equation should be rearranged such that all the interface variables and non-interface variables are separated which results in the following system of equations:

$$\begin{bmatrix} K_1^1 & \cdots & K_1^{k-1} & K_1^{l+1} & \cdots & K_1^n & K_1^k & \cdots & K_1^l \\ K_2^1 & \cdots & K_2^{k-1} & K_2^{l+1} & \cdots & K_2^n & K_1^k & \cdots & K_2^l \\ \vdots & \ddots & \vdots & \vdots & \ddots & \vdots & \vdots & \ddots & \vdots \\ K_{n-1}^1 & \cdots & K_{n-1}^{k-1} & K_{n-1}^{l+1} & \cdots & K_{n-1}^n & K_1^k & \cdots & K_{n-1}^l \\ K_n^1 & \cdots & K_n^{k-1} & K_n^{l+1} & \cdots & K_n^n & K_1^k & \cdots & K_n^l \end{bmatrix} \times \begin{Bmatrix} u_1 \\ \vdots \\ u_{k-1} \\ u_{l+1} \\ \vdots \\ u_n \\ u_k \\ \vdots \\ u_l \end{Bmatrix} = \begin{Bmatrix} F_1 \\ \vdots \\ F_{k-1} \\ F_{l+1} \\ \vdots \\ F_n \\ F_k \\ \vdots \\ F_l \end{Bmatrix} \tag{37}$$

The above obtained equations can be expressed as the following matrix form:

$$\begin{bmatrix} \mathbf{K}_{oo} & \mathbf{K}_{oi} \\ \mathbf{K}_{io} & \mathbf{K}_{ii} \end{bmatrix} \begin{Bmatrix} \mathbf{u}_{F_o} \\ \mathbf{u}_{F_i} \end{Bmatrix} = \begin{Bmatrix} \mathbf{F}_{F_o} \\ \mathbf{F}_{F_i} \end{Bmatrix} \tag{38}$$

where $\mathbf{u}_{F_i}$ is the interface variables in the FEM sub-domain and $\mathbf{u}_{F_i} = [u_k, u_{k+1}, \ldots, u_l]^T$; $\mathbf{u}_{F_o}$ denotes the non-interface variables in the FEM subdomain. $\mathbf{K}_{oo}$, $\mathbf{K}_{oi}$, $\mathbf{K}_{io}$, $\mathbf{K}_{ii}$, $\mathbf{F}_{F_o}$ and $\mathbf{F}_{F_i}$ are the corresponding matrices and vectors.

### 3.2. Formulations of BEM domain

Based on the nodal locations shown in Fig. 5(a), the matrices ($\mathbf{H}$, $\mathbf{G}$, $\mathbf{u}$ and $\mathbf{t}$) of linear algebraic equations in Eq. (34) can be expressed as

$$\mathbf{H} = \begin{bmatrix} H_1^1 & \cdots & H_1^{k-1} & H_1^k & \cdots & H_1^l & H_1^{l+1} & \cdots & H_1^n \\ H_2^1 & \cdots & H_2^{k-1} & H_2^k & \cdots & H_2^l & H_1^{l+1} & \cdots & H_2^n \\ \vdots & \ddots & \vdots & \vdots & \ddots & \vdots & \vdots & \ddots & \vdots \\ H_{n-1}^1 & \cdots & H_{n-1}^{k-1} & H_{n-1}^k & \cdots & H_{n-1}^l & H_1^{l+1} & \cdots & H_{n-1}^n \\ H_n^1 & \cdots & H_n^{k-1} & H_n^k & \cdots & H_n^l & H_1^{l+1} & \cdots & H_n^n \end{bmatrix}, \tag{39}$$

$$\mathbf{G} = \begin{bmatrix} G_1^1 & \cdots & G_1^{k-1} & G_1^k & \cdots & G_1^l & G_1^{l+1} & \cdots & G_1^n \\ G_2^1 & \cdots & G_2^{k-1} & G_2^k & \cdots & G_2^l & G_1^{l+1} & \cdots & G_2^n \\ \vdots & \ddots & \vdots & \vdots & \ddots & \vdots & \vdots & \ddots & \vdots \\ G_{n-1}^1 & \cdots & G_{n-1}^{k-1} & G_{n-1}^k & \cdots & G_{n-1}^l & G_1^{l+1} & \cdots & G_{n-1}^n \\ G_n^1 & \cdots & G_n^{k-1} & G_n^k & \cdots & G_n^l & G_1^{l+1} & \cdots & G_n^n \end{bmatrix}, \tag{40}$$

$$\mathbf{u} = \begin{bmatrix} u_1 & \cdots & u_{k-1} & u_k & \cdots & u_l & u_{l+1} & \cdots & u_n \end{bmatrix}^T \tag{41}$$

and

$$\mathbf{t} = \begin{bmatrix} t_1 & \cdots & t_{k-1} & t_k & \cdots & t_l & t_{l+1} & \cdots & t_n \end{bmatrix}^T \tag{42}$$

Separating the interface variables ($\mathbf{u}_{Bi}$ and $\mathbf{t}_{Bi}$) from the non-interface variables ($\mathbf{u}_{Bo}$ and $\mathbf{t}_{Bo}$), we can obtain the following equations

$$\begin{bmatrix} \mathbf{H}_{ii} & \mathbf{H}_{io} \\ \mathbf{H}_{oi} & \mathbf{H}_{oo} \end{bmatrix} \begin{Bmatrix} \mathbf{u}_{Bi} \\ \mathbf{u}_{Bo} \end{Bmatrix} = \begin{bmatrix} \mathbf{G}_{ii} & \mathbf{G}_{io} \\ \mathbf{G}_{oi} & \mathbf{G}_{oo} \end{bmatrix} \begin{Bmatrix} \mathbf{t}_{Bi} \\ \mathbf{t}_{Bo} \end{Bmatrix} \tag{43}$$

where $\mathbf{H}_{ii}$, $\mathbf{H}_{io}$, $\mathbf{H}_{oi}$, $\mathbf{H}_{oo}$, $\mathbf{G}_{ii}$, $\mathbf{G}_{io}$, $\mathbf{G}_{oi}$ and $\mathbf{G}_{oo}$ are the re-constructed matrices and vectors corresponding to the interface variables and non-interface variables.

Through partial eliminations, the system equation in Eq. (43) can further be transformed to

$$\begin{bmatrix} \mathbf{A}_{ii} & 0 \\ \mathbf{A}_{oi} & \mathbf{A}_{oo} \end{bmatrix} \begin{Bmatrix} \mathbf{u}_{Bi} \\ \mathbf{u}_{Bo} \end{Bmatrix} = \begin{bmatrix} \mathbf{B}_{ii} & \mathbf{B}_{io} \\ \mathbf{B}_{oi} & \mathbf{B}_{oo} \end{bmatrix} \begin{Bmatrix} \mathbf{t}_{Bi} \\ \mathbf{t}_{Bo} \end{Bmatrix} \tag{44}$$

Then, the equations relating to the interface quantities can be expressed as

$$\mathbf{A}_{ii}\mathbf{u}_{Bi} = \mathbf{B}_{ii}\mathbf{t}_{Bi} + \mathbf{B}_{io}\mathbf{t}_{Bo} \tag{45}$$

From Eq. (45), it is easy to obtain the following relationships

$$\mathbf{t}_{Bi} = \mathbf{B}_{ii}^{-1}\mathbf{A}_{ii}\mathbf{u}_{Bi} - \mathbf{B}_{ii}^{-1}\mathbf{B}_{io}\mathbf{t}_{Bo} \tag{46}$$

### 3.3. Formulations of coupling scheme

It is noteworthy that the basic algebraic equations in Eq. (38) for FEM are formulated in terms of temperatures ($\mathbf{u}_{Fi}$ and $\mathbf{u}_{Fo}$) and thermal loads ($\mathbf{F}_{Fi}$ and $\mathbf{F}_{Fo}$), while those in BEM are temperatures ($\mathbf{u}_{Bi}$ and $\mathbf{u}_{Bo}$) and heat fluxes ($\mathbf{t}_{Bi}$ and $\mathbf{t}_{Bo}$). Here, the heat fluxes $\mathbf{t}_{Bi}$ should be converted into the equivalent thermal loads ($\mathbf{F}_{Fi}$) by following formulation

$$\mathbf{F}_{B_i} = \mathbf{M}_B\mathbf{t}_{B_i} = \mathbf{K}_{B_i}\mathbf{u}_{B_i} - \bar{\mathbf{R}}_{B_i} \tag{47}$$

and

$$\mathbf{K}_{B_i} = \mathbf{M}_B\mathbf{B}_{ii}^{-1}\mathbf{A}_{ii}, \tag{48}$$

$$\bar{\mathbf{R}}_{B_i} = \mathbf{M}_B \mathbf{B}_{ii}^{-1} \mathbf{B}_{io} \mathbf{t}_{Bo}, \tag{49}$$

where the transformation matrix $\mathbf{M}_B$ can be found in [48]. And the Eq. (47) can further be written as

$$\begin{bmatrix} 0 & 0 \\ 0 & \mathbf{K}_{B_i} \end{bmatrix} \begin{Bmatrix} \mathbf{u}_{F_o} \\ \mathbf{u}_{B_i} \end{Bmatrix} = \begin{Bmatrix} 0 \\ \mathbf{F}_{B_i} + \bar{\mathbf{R}}_{B_i} \end{Bmatrix}. \tag{50}$$

As we all know, the compatibility conditions must be satisfied along the interface between the FEM subdomain and BEM subdomain, which means the temperatures ($\mathbf{u}$) calculated for the two domains are equal. A similar relationship remains for the equilibrium condition along the interface, except that a negative sign must be given to account for the opposite directions of the outward boundary normal in the two domains. These conditions produce the following relationships along the interface of FEM subdomain and BEM subdomain

$$\mathbf{u}_{F_i} = \mathbf{u}_{B_i}; \ \mathbf{F}_{F_i} = -\mathbf{F}_{B_i}. \tag{51}$$

Adding Eqs. (38) and (50), we can obtain the following coupling equation:

$$\begin{bmatrix} \mathbf{K}_{oo} & \mathbf{K}_{oi} \\ \mathbf{K}_{io} & \mathbf{K}_{ii} + \mathbf{K}_{B_i} \end{bmatrix} \begin{Bmatrix} \mathbf{u}_{F_o} \\ \mathbf{u}_{F_i} \end{Bmatrix} = \begin{Bmatrix} \mathbf{F}_{F_o} \\ \bar{\mathbf{R}}_{B_i} \end{Bmatrix}. \tag{52}$$

It should be noted that the matrix $\mathbf{K}_{B_i}$ from BEM is fully populated and asymmetric, which destroys the sparsity of the FE stiffness matrix. Therefore, the whole coefficient matrix on the left side of Eq. (52) will be symmetrized, by adding the Eq. (52) and following Eq. (53)

$$\begin{bmatrix} 0 & 0 \\ 0 & \mathbf{K}_l - \mathbf{K}_{B_i} \end{bmatrix} \begin{Bmatrix} \mathbf{u}_{F_o} \\ \mathbf{u}_{F_i} \end{Bmatrix} = \begin{Bmatrix} 0 \\ \mathbf{K}_l - \mathbf{K}_{B_i} \end{Bmatrix} \begin{Bmatrix} \mathbf{u}_{F_i} \end{Bmatrix} \tag{53}$$

Finally, a coupling equation with symmetric coefficient matrix will be obtained

$$\begin{bmatrix} \mathbf{K}_{oo} & \mathbf{K}_{oi} \\ \mathbf{K}_{io} & \mathbf{K}_{ii} + \mathbf{K}_l \end{bmatrix} \begin{Bmatrix} \mathbf{u}_{F_o} \\ \mathbf{u}_{F_i} \end{Bmatrix} = \begin{Bmatrix} \mathbf{F}_{F_o} \\ \bar{\mathbf{R}}_{B_i} \end{Bmatrix} + \begin{Bmatrix} 0 \\ \mathbf{K}_l - \mathbf{K}_{B_i} \end{Bmatrix} \begin{Bmatrix} \mathbf{u}_{F_i} \end{Bmatrix} \tag{54}$$

where

$$\mathbf{K}_l = \frac{1}{2} \left( \mathbf{K}_{B_i}^T + \mathbf{K}_{B_i} \right). \tag{55}$$

The temperatures (including the interface temperatures $\mathbf{u}_{Fi}$) in the FEM sub-domain can be obtained by solving the above coupling equation. According to boundary conditions (the $\mathbf{u}_{Bi} = \mathbf{u}_{Fi}$ along the interface), the boundary quantities of the BEM sub-domain can be obtained by solving the linear equations for BEM part. And the internal temperature at any point $p$ in the BEM sub-domain ($p \in \Omega^B$) can be obtained by the following internal boundary integral equation

$$u(p) = \int_{\Gamma_{\mathrm{BEM}}} t(\mathbf{x}) U(\mathbf{y}, \mathbf{x}) d\Gamma(\mathbf{x}) - \int_{\Gamma_{\mathrm{BEM}}} u(\mathbf{x}) T(\mathbf{y}, \mathbf{x}) d\Gamma(\mathbf{x}) \tag{56}$$

## 4. Implementation of the coupling scheme by ABAQUS

The ABAQUS software, which provides abundant element libraries and material model libraries, is currently one of the most powerful finite element analysis tool in the world. The user element subroutine (UEL) provided by ABAQUS has gained considerable prominence due to the flexibility of defining a new finite element. This function of ABAQUS is intended for advanced users. It will require considerable coding by the user/developer even for some simple test examples. The UEL will be called for each element that is of a general user-defined element type each time element calculations are required and must perform all of the calculations for the element, appropriate to the current activity in the analysis. The user subroutine interface for UEL can be found in the ABAQUS documentation [49].

In this section, we will introduce the implementation of the proposed coupling scheme.

Firstly, the model needs to be divided into two parts according to the geometric information or material properties (as shown in Fig. 4). It should be pointed out that when the small-scale part, thin section or coating is regarded as the BE part, some nearly singular integral schemes should be adopted to solve the large number of nearly singular integrals [50]. Then, the FE part needs to be discretized into several quadrilateral or triangular finite elements by the pre-process of ABAQUS (shown in Fig. 5(b)). And the BE part should be divided into typical boundary elements on the boundary or surface (shown in Fig. 5(a)).

Two deformable parts should be built by the ABAQUS: one is the FE part, and the other is the new-BE part. It is not difficult to understand for the FE part as shown in the right hand side of Fig. 6(a), which is a standard operation for ABAQUS. The new-BE part means the BE part is defined as a 1D simplified FE part (see the left of Fig. 6(a)). And the new-BE part should be meshed into several boundary elements. The number of nodes along the interface for the new-BE part must be equal to that of FEM part. As shown in Fig. 6(b), the two parts built by ABAQUS are connected by the command 'tie'.

The overall treatment for the current coupling scheme is summarized in Fig. 7. As shown in Fig. 7, the model is divided into two parts: the FE part and BE part. A self-written BE code is used to obtain the effective stiffness matrix $\mathbf{K}_{Bi}$ and effective fluxes $\mathbf{F}_{Bi}$ for the interface. And the FE part will be preprocessed by ABAQUS. Then, the input file obtained from ABAQUS will be edited to define a unique user element for the closed BE domain. Here, the user element is regarded as a super-element including all nodes along the interface between the FE and BE sub-domains, but no internal nodes at all. Then the new input file will be included in the ABAQUS and the user subroutine with BEM program is called to compute the temperatures and flux of the FE part. Then the user subroutine URDFIL is used to extract the temperature and flux at the interface and pass them to BEM program to obtain all the temperature and flux for the BE part.

## 5. Numerical examples

In this section, through several numerical examples, the accuracy and effectiveness of the proposed coupling scheme for heat transfer problems are demonstrated. The first example focuses on the accuracy analysis of the proposed coupling scheme. To verify the effectiveness of the present method for the analysis of multi-scale model, a model with multi-scale structures is studied in the second example. And the computation time comparison between the proposed coupling method and ABAQUS is given in the third example.

### 5.1. Heat transfer through plane wall with thin structures

In practice, we often encounter plane walls that consist of thin structures. As shown in Fig. 8, consider an $a \times a$ substrate with thermal conductivity 22 W/m K. The left side is covered by a ceramic coating structure with thermal conductivity 2.3 W/m K, which provides the thermal insulation. The thickness of the coating is $\delta = 0.1$ m and the geometry of the substrate $a = 1$ m. The temperature on the left side of the coating is specified as 150 °C. And the heat flux $q$ on the right side of the substrate is fixed as 100 W/m$^2$. All the upper and lower boundaries are insulated, i.e. $\Delta T \cdot \mathbf{n} = \mathbf{0}$. In the computation, BEM is used to study the substrate (right part in Fig. 8) and FEM is used to analyze the coating structure (left part in Fig. 8).

Fig. 9(a) shows the mesh used in the coupling method. In the computation, 40 surface (quadrilateral) elements are used for FE part (coating structure) and 40 boundary elements is used in the BE part (substrate). It should be pointed out that two parts are needed to be established by the ABAQUS. The first part is the coating structure, as shown the FE part (left) in Fig. 9(b). To build the relationship of FE and BE parts, boundary elements (the line) shown in right part of Fig. 9(b) is also needed to build by the ABAQUS. Then, the two discretization areas will be tied together by the 'tie' command in ABAQUS, as shown in Fig. 9(b).

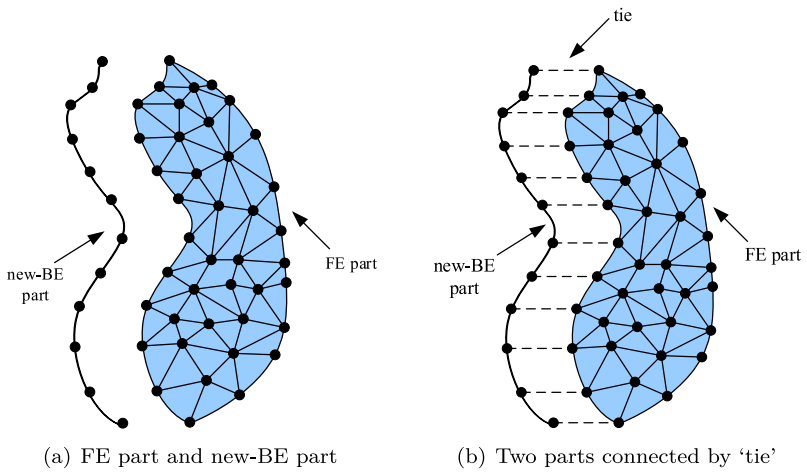


**Fig. 6.** Model built by ABAQUS.

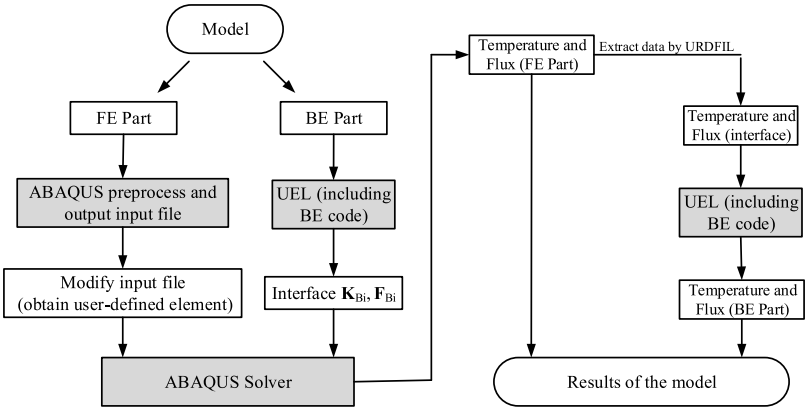


**Fig. 7.** The flowchart of coupling scheme.

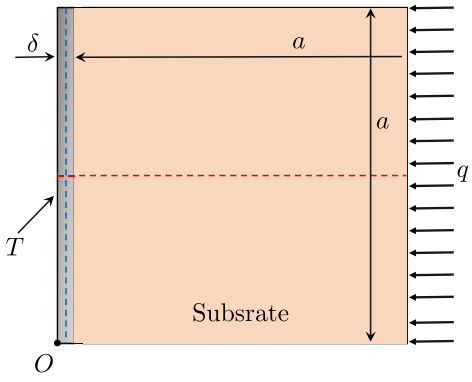


**Fig. 8.** Heat transfer through a model with flat coating. (For interpretation of the references to color in this figure legend, the reader is referred to the web version of this article.)

Here, a very refined finite element model is constructed with the FEM software ABAQUS to offer a reference solution. 11,000 DC2D4 elements and 11 312 nodes are used in the model, where the edge length of the elements is 0.01. Figs. 10(a) and 10(b) show temperature contour plots of the FE region for the coupling method and reference temperature, respectively. As shown in Fig. 10(a), a red sign is added to the upper right corner which represents the location of the user defined element in ABAQUS. One can find that the results obtained by the coupling method have a good agreement with the reference solutions.

To carry out the accuracy analysis, the following relative error is defined

$$\text{Relative error(RE)} = \frac{|f_{\text{num}} - f_{\text{ref}}|}{|f_{\text{ref}}|} \tag{57}$$

where $f_{\text{num}}$ and $f_{\text{ref}}$ represent the numerical solution and reference solution, respectively.

To illustrate the accuracy of the current scheme, a set of points is distributed along curve $C_1$ (red line in Fig. 8) with definition

$$C_1 = \{(x, y) : 0 \le x \le (\delta + a), y = a/2\}. \tag{58}$$

Fig. 11(a) compares the temperature distribution along the curve $C_1$ obtained using the present scheme and a reference solution. In Fig. 11(a), the number of degree of freedom (ndof) is the sum of ndof of FE part and BE part. The relative errors of the temperature for different ndof are presented in Fig. 11(b), from which we can find that the maximum error occurs in the location of interface boundary between FE part and BE part.

Here, the interface boundary of the BE part and FE part is defined as $C_2$ with

$$C_2 = \{(x, y) : x = \delta, 0 \le y \le a\}. \tag{59}$$

The temperature distribution and relative error along the interface $C_2$ are shown in Figs. 12(a) and 12(b), respectively. As one can observe, there is drastic fluctuation for the results of temperature along the interface. From Figs. 12(a) and 12(b) we can observe that the results will tend towards stability with the increase of ndof. And the relative errors of obtained temperature also reduce with the increase of the ndof.

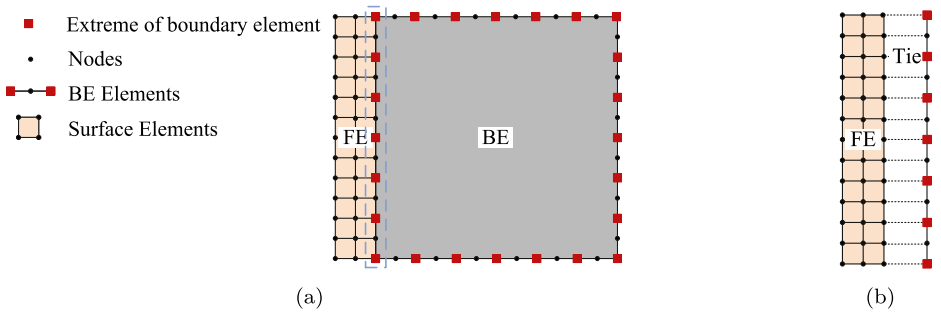


**Fig. 9.** Diagrammatic sketch of meshes (a) Meshes of FE and BE parts; (b) Connections part shown in the slight blue rectangular in (a). (For interpretation of the references to color in this figure legend, the reader is referred to the web version of this article.)

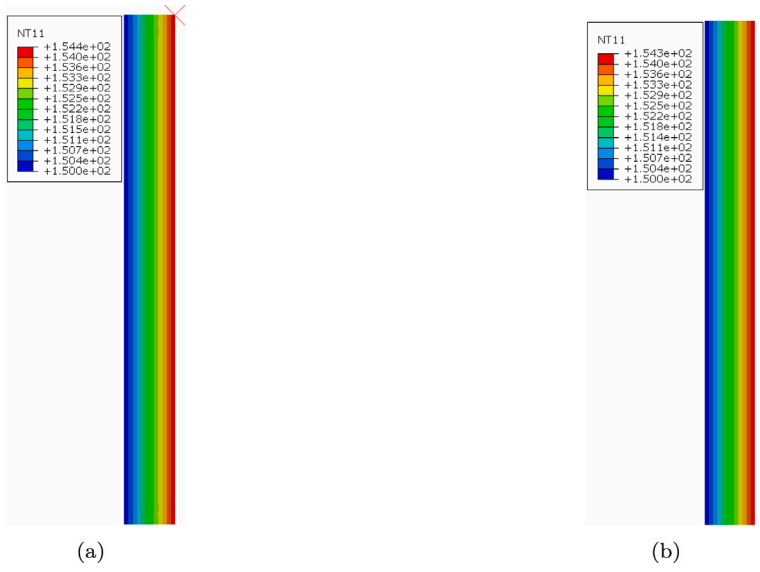


**Fig. 10.** Temperature contour plots of different methods (a) Results obtained by current coupling method; (b) Reference results.

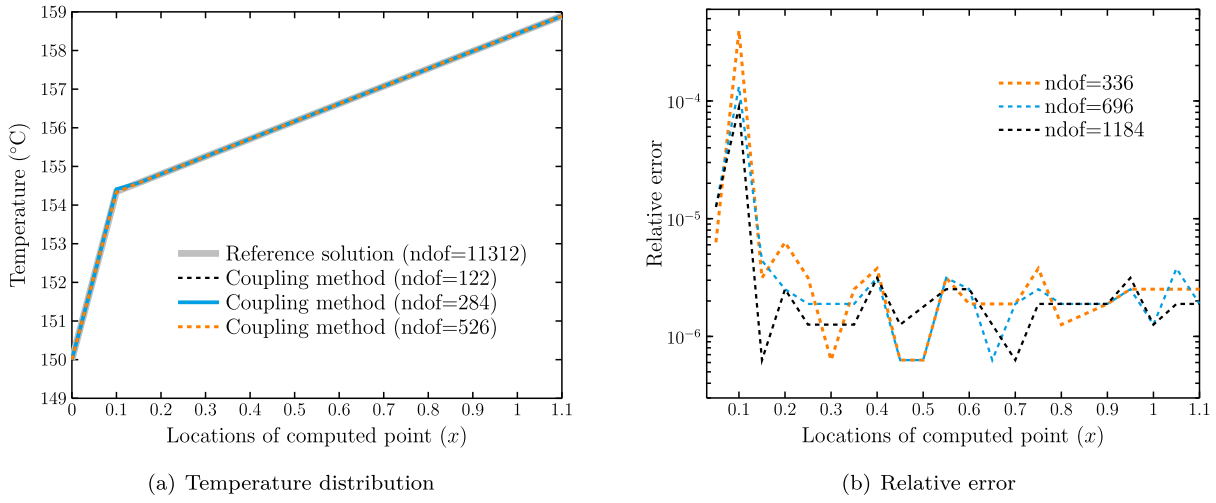


**Fig. 11.** The temperature and relative error obtained by the coupling method for different ndof along the line $C_1$.

Figs. 13(a) and 13(b) present the temperature distributions and the corresponding relative error of temperature along the line $C_3$ (blue line in Fig. 8) for different ndof. The line $C_3$ is defined as

$$C_3 = \{(x, y) : x = \delta/2, 0 \le y \le a\}. \tag{60}$$

Fig. 14 shows us the temperature distribution along the curve $y = 0.5$ m when different number of element is used. In the computation, the ndof used by FEM is fixed as 603 and the ndof of BEM varies from 1201 to 2995. From Fig. 14, we can find that the temperature obtained by the coupling scheme is stable with the ndof changing from 1201 to 2995. Some thinner structures are calculated in Fig. 15, from which we can clearly see that the current solutions are in good agreement with the reference results even when $\delta = 10^{-3}$ m.

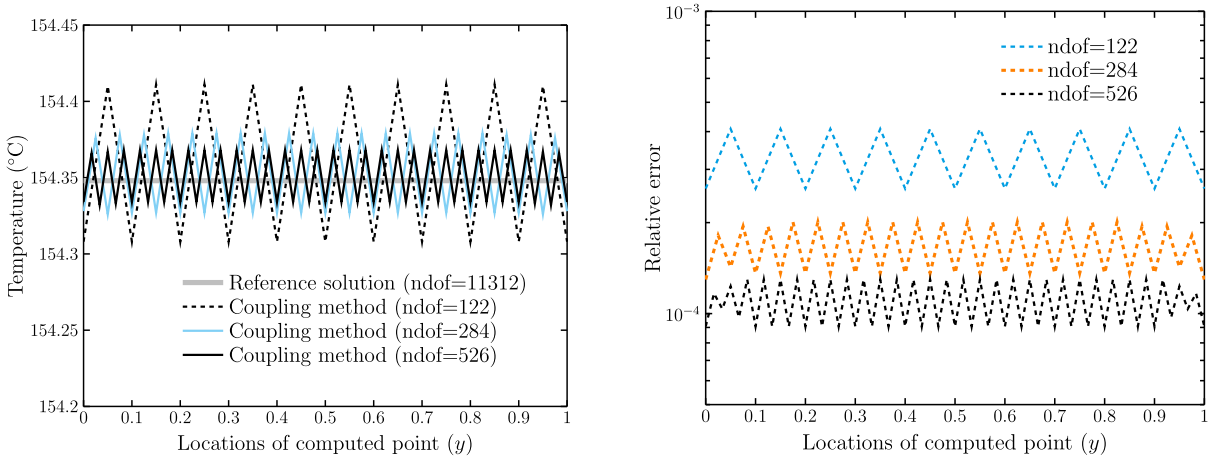


(a) Temperature distribution (b) Relative error

**Fig. 12.** The temperature and relative error along the interface $C_2$.

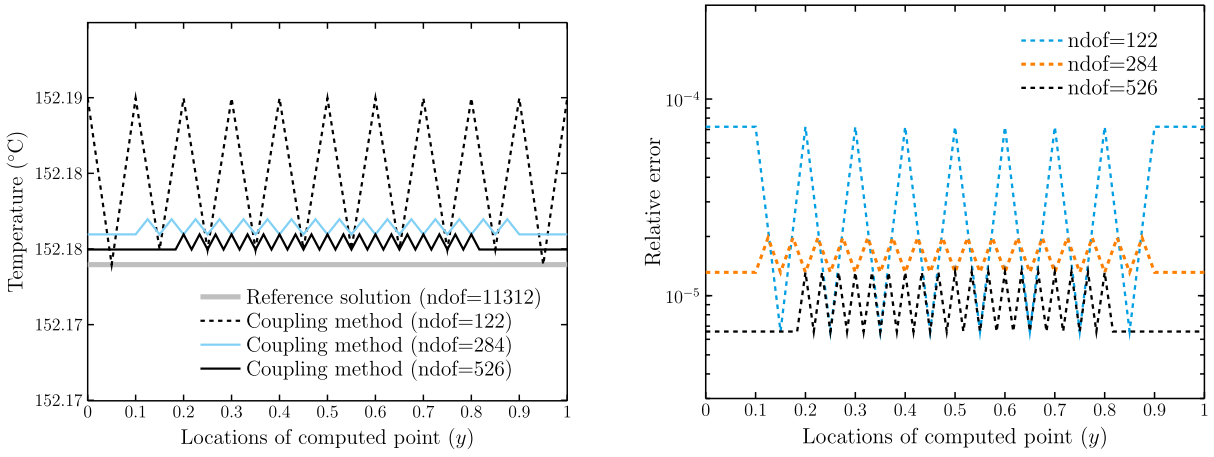


(a) Temperature distribution (b) Relative error

**Fig. 13.** The temperature and relative error along the curve $C_3$.

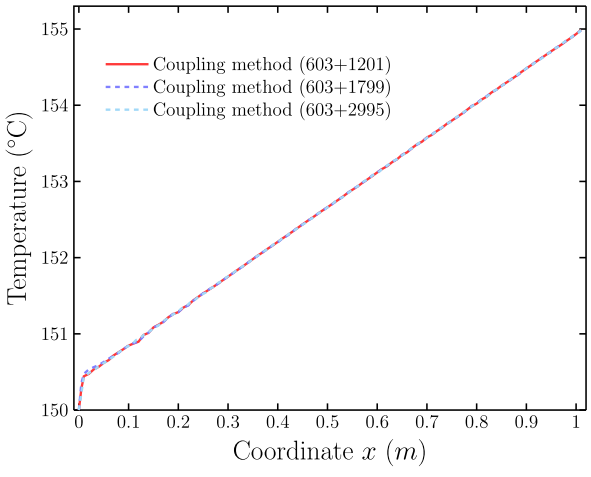


**Fig. 14.** Temperatures obtained by current scheme for different ndof.

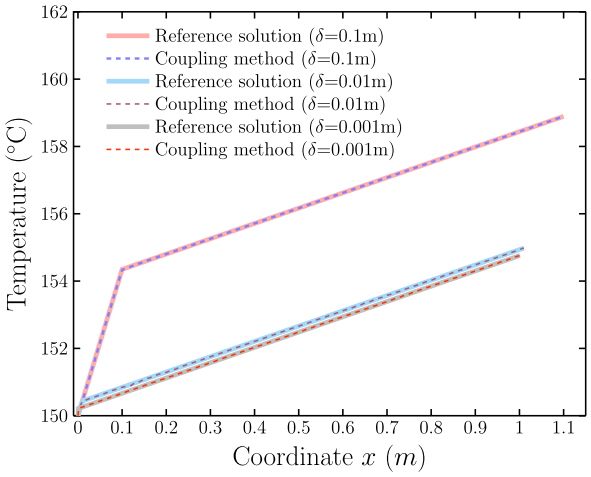


**Fig. 15.** Temperatures along the curve $y = 0.5$ m for different thickness $\delta$.

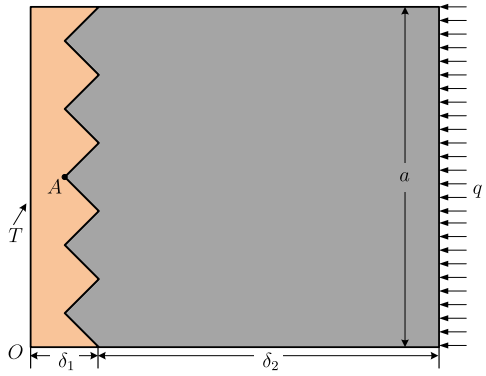


**Fig. 16.** Heat transfer model.

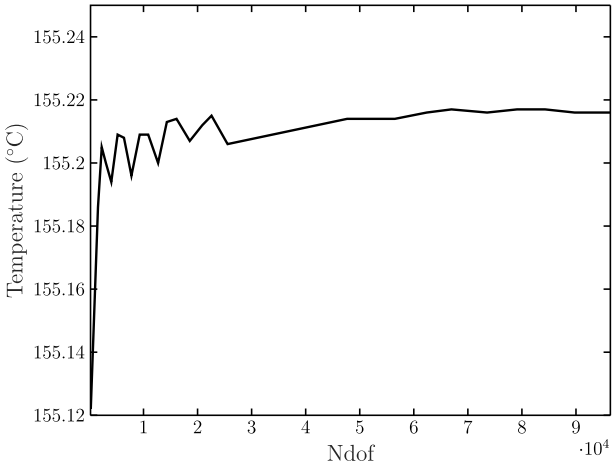


**Fig. 17.** The temperature at point $A$ obtained by ABAQUS.

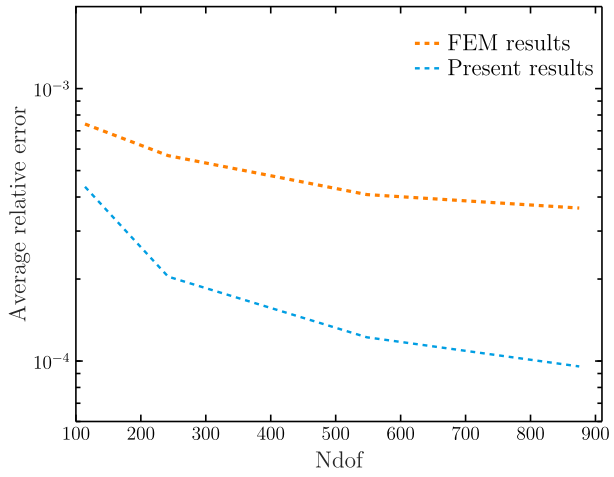


**Fig. 18.** Average relative errors obtained by two methods.

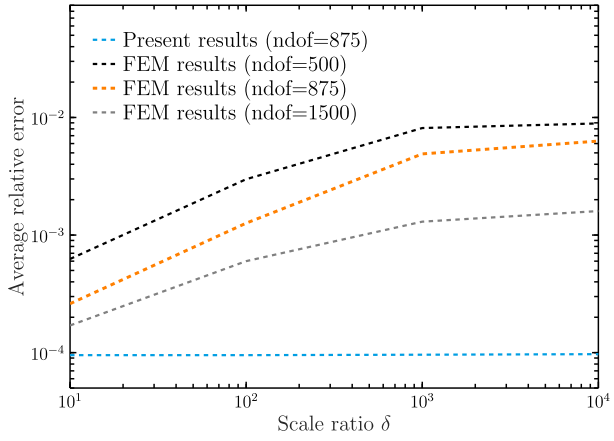


**Fig. 19.** Average relative errors of temperature for different scale ratio $\delta$.

### 5.2. Heat transfer through multi-scale structures with serrated interface

In the second example, a heat transfer problem with serrated interface is studied as shown in Fig. 16. The conductivity of the right substrate is taken as 22 W/m K and the size of the substrate is $a \times \delta_2$. As shown in the figure, the left side of the substrate is covered with a coating of thickness $\delta_1$ and having thermal conductivity 2.3 W/m K. In the computation, the parameters $a$ and $\delta_1$ are fixed as 1 m and 0.1 m, respectively. And the length $\delta_2$ of substrate varies from 1 m to $10^3$ m. Therefore, the scale ratio $\delta$ of the model will vary from 10 to $10^4$. The scale ratio $\delta$ is defined as

$$\delta = \frac{\delta_2}{\delta_1}. \tag{61}$$

Fig. 17 shows the temperature obtained by ABAQUS at point $A$ (shown in Fig. 16) when different ndof is used. From the figure, we can see that the values of temperature tends to be stable when ndof reaches 50 000. Therefore, the stable value of temperature will be adopted as the reference solution in this example.

For this problem, an analytical solution is not available, and the convergence of the problem is established by taking a very refined ABAQUS model as the reference solution. Thus, we define an error metric

$$\text{Average relative error (ARE)} = \frac{1}{N}\sum_{n=1}^{N}\left|\frac{T_n - T_{ref}}{T_{ref}}\right| \tag{62}$$

where $N$ is the number of the nodes used in the computation; $T_n$ represents the temperature of the $n$th node and $T_{\text{ref}}$ is the reference temperature at the corresponding node. In this example, the $T_{\text{ref}}$ is taken as the stable value of temperature as shown in Fig. 17.

The average relative errors (ARE) of temperatures along the serrated interface obtained by the coupling scheme and FEM are given in Fig. 18. Here, the $N$ used in the ARE (in Eq. (62)) is selected as 21, 41, 61 and 81. From Fig. 18, we can observe that the two methods can obtain accurate results and the convergence can be clearly seen as the ndof increases from 100 to 900. In addition, when same ndof is used in the coupling scheme and FEM, the results obtained by the coupling scheme is more accurate.

Fig. 19 shows the behavior of the AREs of interface temperature obtained by present coupling method and FEM as the scale ratio increases from 10 to $10^4$. Again, the coupled method can still deliver higher accuracy of results than FEM even when ndof=1500 is used in FEM. From Fig. 19, we can also find that the AREs obtained by the coupled method remain stable for different scale ratio.

### 5.3. Heat transfer through a practical model

A ball grid array (BGA) is a kind of surface mount package which is used in electronic products to mount integrated circuits. In our final example, shown in Fig. 20, a part of BGA including solder ball, Cu pad and printed circuit board (PCB) is considered. The geometry parameters of the considered model is given as $l_1 = 3$ mm, $h_1 = 0.2$ mm, $l_2 = l_3 = 1$ mm, $h_2 = h_3 = 0.05$ mm, $R = 94.325$ mm. The thermal conductivities of the solder ball, Cu pad and PCB are taken as 67 W/m K, 397 W/m K and

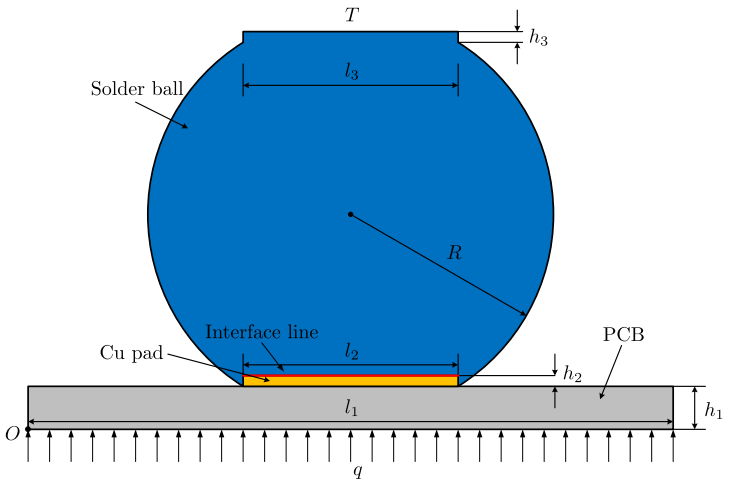


**Fig. 20.** Sketch of the BGA. (For interpretation of the references to color in this figure legend, the reader is referred to the web version of this article.)

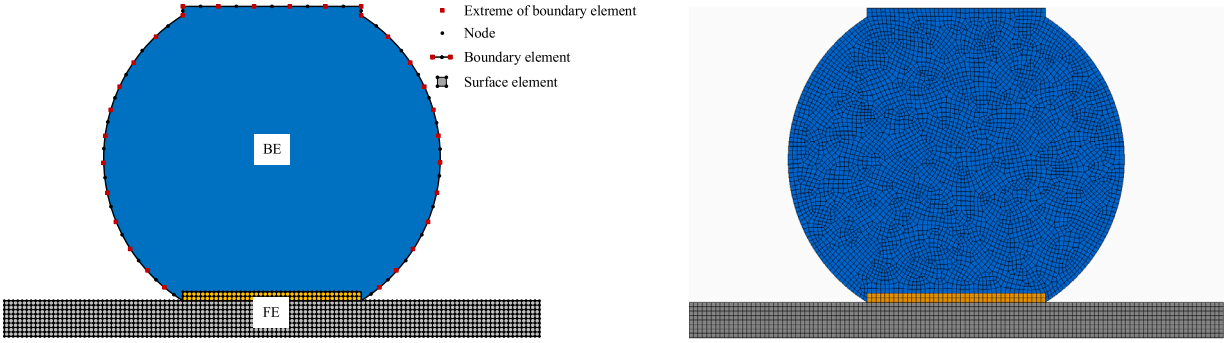


(a) Mesh used in the coupling scheme (b) Mesh used by the FEM (ndof=6204)

**Fig. 21.** Meshes used in different methods.

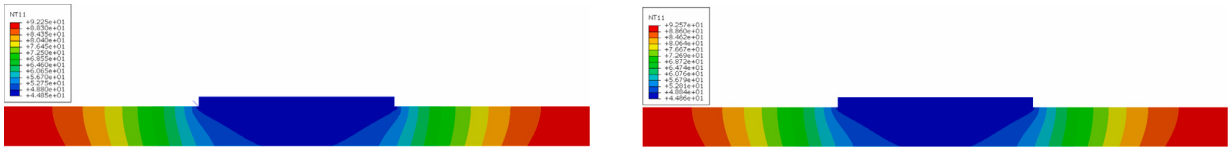

(a) Results obtained by current coupling scheme (b) Reference results obtained by a refined FEM model (ndof=26273)

**Fig. 22.** Temperature distribution for different methods.

6.5 W/m K. The temperature on the topside and the heat flux on the bottom edge are prescribed as boundary conditions, being $T = 40$ °C and $q = 0.1$ W/m$^2$. All the left and right boundaries are insulated, i.e. $\Delta T \cdot \mathbf{n} = 0$.

Fig. 21(a) shows the meshes used in the proposed coupling scheme. As shown in the figure, we will use BEM to calculate the solder ball, and use FEM to analyze the Cu pad and PCB. Fig. 21(b) gives one of the meshes used by the FEM. From the two figures, we can observe that the number of element can be reduced by the proposed coupling scheme.

Figs. 22(a) and 22(b) show the temperature contour plots of different methods, from which the temperature distribution on the Cu pad and PCB field can be seen clearly. Figs. 22(a) and 22(b) also imply that the accuracy of the present method is satisfactory in the whole field of the problem. Fig. 23 presents the temperature distribution along the interface line (displayed in red in Fig. 20), for different model sizes. The reference solutions are obtained from a very refined FEM model consisting of 24 435, 26 273 and 55 000 nodes. From Fig. 23, it can be seen that when ndof = 242, the results obtained by the coupling scheme are satisfactory.

In Table 1, the computation time of different analysis methods is given with different nodfs. When the accuracy of results is similar for the coupling method and FEM, the number of degree freedom used in the coupling method is much smaller than that used in the FEM. From Table 1, it can be seen that the computational times of the two methods is increased with the increasing of ndof. However, since less ndof is used in the coupled method, the computation time of the coupling is largely reduced. Thus, the considerably superior computational efficiency of the coupled method can be observed from this Table 1.

## 6. Conclusions

In this paper, a FEM-BEM coupling method, which might be effective for multi-scale structures is used to study the steady-state heat transfer problem. A major attraction of this coupling method is that the self-written BEM-code, which is started inside UEL, is integrated into the FE systems as a user defined finite super-element. The effective

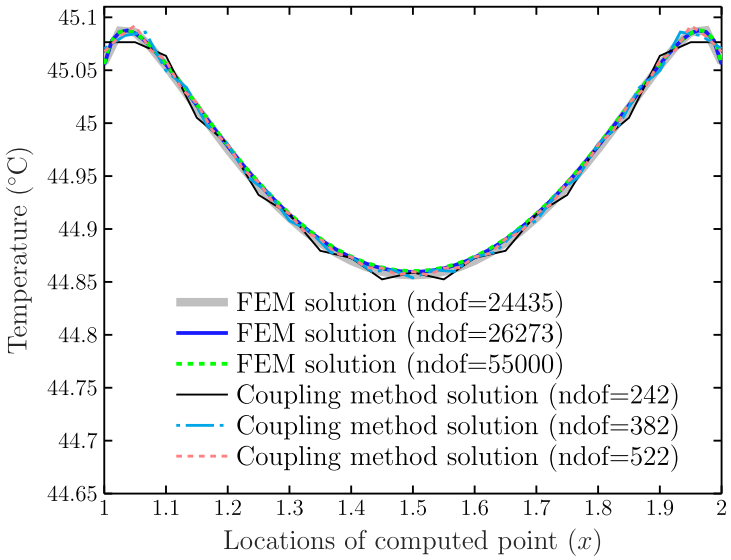


**Fig. 23.** Temperature distribution along the interface line (red line in Fig. 20) obtained by the proposed method and FEM.

**Table 1**
Comparisons of computation time for different methods.

| Methods | ndof | User input processing | | Analysis processing | |
|---|---|---|---|---|---|
| | | CPU time (s) | Wall-clock time (s) | CPU time (s) | Wall-clock time (s) |
| FEM (ABAQUS) | 24 435 | 3.2 | 3 | 2.5 | 3 |
| | 26 273 | 3.5 | 4 | 2.7 | 3 |
| | 55 000 | 7 | 7 | 5.8 | 7 |
| Coupled method | 616 | 0.3 | 1 | 0.8 | 1 |
| | 916 | 0.5 | 1 | 1.5 | 2 |
| | 1216 | 0.7 | 1 | 3.1 | 3 |

stiffness and effective fluxes along the interface of BE and FE subdomains are obtained by the self-written BE code and handled as the given boundary conditions for the FEM part. By using the advantages of finite and boundary elements and avoiding their respective disadvantages, the efficiency and accuracy of the coupling scheme is improved. A range of numerical examples together demonstrate that the proposed scheme delivers highly accurate solutions in a computationally efficient manner in the solution of heat transfer problems.

Based on the powerful platform of the ABAQUS, the proposed coupling scheme will be further developed for a more detailed simulation of engineering problems with multi-scale structures.

## Acknowledgments

The research was supported by the National Natural Science Foundation of China (Nos. 12002009, 11872078), the General Program of Science and Technology Development Project of Beijing Municipal Education Commission, China (No. KM202110005032), Beijing Postdoctoral Research Foundation and General Program of Science and Technology Development Project of BJUT, China.

## References

[1] Cui Y, Qin Z, Wu H, Li M, Hu Y. Flexible thermal interface based on self-assembled boron arsenide for high-performance thermal management. Nature Commun 2021;12:1284.
[2] Lee KY, Lee TS. Hygrothermal fracture analysis of plastic IC package in reflow soldering process. J Electron Packag 1999;121(3):148–55.
[3] Yang J, Hu H, Potier-Ferry M. Least−square collocation and lagrange multipliers for taylor meshless method. Numer Methods Partial Differential Equations 2019;35(1):84–113.
[4] Raszkowski T, Zubert M. Analysis of algorithm efficiency for heat diffusion at nanoscale based on a MEMS structure investigation. Energies 2020;13(10):2520.
[5] Brebbia CA, Telles JCF, Wrobel LC. Boundary element techniques: theory and applications in engineering. Springer Science & Business Media; 2012.
[6] Prosper D, Kausel E. Wave scattering by cracks in laminated media. In: International conference in computational engineering & sciences (ices). Puerto Vallarta, Mexico; 2001.
[7] Wang F, Fan C-M, Hua Q, Gu Y. Localized MFS for the inverse Cauchy problems of two-dimensional Laplace and biharmonic equations. Appl Math Comput 2020;364:124658.
[8] Lim NREG, Ubando AT, Gonzaga JA, Dimagiba RRN. Finite element analysis on the factors affecting die crack propagation in bga under thermo-mechanical loading. Eng Fail Anal 2020;116:104717.
[9] Krondorfer R, Kim YK, Kim J, Gustafson C-G, Lommasson TC. Finite element simulation of package stress in transfer molded MEMS pressure sensors. Microelectron Reliab 2004;44(12):1995–2002.
[10] Vallepuga-Espinosa J, Ubero-Martínez I, Rodríguez-Tembleque L, Cifuentes-Rodríguez J. A boundary element procedure to analyze the thermomechanical contact problem in 3d microelectronic packaging. Eng Anal Bound Elem 2020;115:28–39.
[11] Vermeersch B, Mey GD. BEM calculation of the complex thermal impedance of microelectronic devices. Eng Anal Bound Elem 2007;31(4):289–98.
[12] Yun C-S, Malberti P, Ciappa M, Fichtner W. Thermal component model for electrothermal analysis of IGBT module systems. IEEE Trans Adv Packag 2001;24(3):401–6.
[13] Huang J, He Z, Li C, Zhao L, Lu X. Heat dissipation optimization and prediction for three-dimensional fan-out package. Int J Therm Sci 2021;166:106983.
[14] Rogié B, Monier-Vinard E, Nguyen M-N, Bissuel V, Laraqi N. Practical analytical modeling of 3D multi-layer printed wired board with buried volumetric heating sources. Int J Therm Sci 2018;129:404–15.
[15] Oda J, Sakamoto J. Applications of FEM for multiple laminated structure in electronic packaging. Finite Elem Anal Des 1998;30(1–2):147–62.
[16] Gong L, Xu Y-P, Ding B, Zhang Z-H, Huang Z-Q. Thermal management and structural parameters optimization of MCM-BGA 3D package model. Int J Therm Sci 2020;147:106120.
[17] Lau C-S, Abdullah M, Che Ani F. Three-dimensional thermal investigations at board level in a reflow oven using thermal-coupling method. Solder Surf Mount Technol 2012;24(3):167–82.
[18] Adams V, Blackburn D, Joshi Y, Berning D. Issues in validating package compact thermal models for natural convection cooled electronic systems. IEEE Trans Compon Packag Manuf Technol: A 1997;20(4):420–31.

[19] Zheng Y-T, Gao X-W, Peng H-F, Xu B-B. The coupled method of multi-domain BEM and element differential method for solving multi-scale problems. Eng Anal Bound Elem 2020;113:145–55.
[20] Khatir Z, Lefebvre S. Boundary element analysis of thermal fatigue effects on high power IGBT modules. Microelectron Reliab 2004;44(6):929–38.
[21] Vermeersch B, Mey GD. BEM calculation of the complex thermal impedance of microelectronic devices. Eng Anal Bound Elem 2007;31(4):289–98.
[22] Guven I, Chan CL, Madenci E. Transient two-dimensional thermal analysis of electronic packages by the boundary element method. IEEE Trans Adv Packag 1999;22(3):476–86.
[23] Dong C, Lee KY. Stress analysis of plastic IC package containing various interface delaminations using the boundary element method. Eng Fract Mech 2008;75(1):1–16.
[24] Yu H, Guo Y, Gong Y, Qin F. Thermal analysis of electronic packaging structure using isogeometric boundary element method. Eng Anal Bound Elem 2021;128:195–202.
[25] Gong YP, Yang HS, Dong CY. A novel interface integral formulation for 3D steady state thermal conduction problem for a medium with non-homogenous inclusions. Comput Mech 2019;63:181–99.
[26] Tadeu A, Simões N, Simões I. Coupling bem/tbem and mfs for the simulation of transient conduction heat transfer. Internat J Numer Methods Engrg 2010;84(2):179–213.
[27] Guven I, Madenci E, Chan CL. Transient two-dimensional heat conduction analysis of electronic packages by coupled boundary and finite element methods. IEEE Trans Compon Packag Technol 2003;25(4):684–94.
[28] Zienkiewicz O, Kelly D, Bettess P. The coupling of the finite element method and boundary solution procedures. Internat J Numer Methods Engrg 1977;11(2):355–75.
[29] Hsiao G, Schnack E, Wendland W. A hybrid coupled finite-boundary element method in elasticity. Comput Methods Appl Mech Engrg 1999;173(3–4):287–316.
[30] Ji D, Lei W, Liu Z. Finite element method and boundary element method iterative coupling algorithm for 2-D elastodynamic analysis. Comput Appl Math 2020;39(218).
[31] Kamiya N, Iwase H. BEM and FEM combination parallel analysis using conjugate gradient and condensation. Eng Anal Bound Elem 1997;20(4):319–26.
[32] He M, Bishop P, Kassab A, Minardi A. A coupled FDM/BEM solution for the conjugate heat transfer problem. Numer Heat Transfer B 1995;28(2):139–54.
[33] Varadarajan A, Sharma K, Singh R. Some aspects of coupled FEBEM analysis of underground openings. Int J Numer Anal Methods Geomech 1985;9(6):557–71.
[34] Rodopoulos DC, Gortsas TV, Polyzos K, Tsinopoulos SV. New BEM/BEM and BEM/FEM scalar potential formulations for magnetostatic problems. Eng Anal Bound Elem 2019;106:160–9.
[35] Dodig H, Poljak D, Cvetković M. On the edge element boundary element method/finite element method coupling for time harmonic electromagnetic scattering problems. Internat J Numer Methods Engrg 2021;122(14):3613–52.
[36] Rodopoulos DC, Gortsas TV, Tsinopoulos SV, Polyzos D. Nonlinear BEM/FEM scalar potential formulation for magnetostatic analysis in superconducting accelerator magnets. Eng Anal Bound Elem 2020;113:259–67.
[37] Deng T, Sheng X, Jeong H, Thompson DJ. A two-and-half dimensional finite element/boundary element model for predicting the vibro-acoustic behaviour of panels with poro-elastic media. J Sound Vib 2021;505:116147.
[38] Bonari J, Marulli MR, Hagmeyer N, Mayr M, Popp A, Paggi M. A multi-scale FEM-BEM formulation for contact mechanics between rough surfaces. Comput Mech 2020;65:731–49.
[39] Liu Z, Majeed M, Cirak F, N. Simpson R. Isogeometric FEM-BEM coupled structural-acoustic analysis of shells using subdivision surfaces. Internat J Numer Methods Engrg 2018;113(9):1507–30.
[40] Wu Y, Dong C, Yang H. Isogeometric FE-BE coupling approach for structural-acoustic interaction. J Sound Vib 2020;481:115436.
[41] Elleithy W, Leong LT. Some recent developments in coupling of finite element and boundary element methods-part II: Dynamic procedures for determining the relaxation parameters for the mixed Dirichlet-Neumann domain decomposition FEM-BEM coupling method. In: Applied mechanics and materials, Vol. 580. Trans Tech Publ; 2014, p. 2943–7.
[42] Bia RA, Ostrowski Z, Kassab AJ, Yin Q, Sciubba E, et al. Coupling BEM,FEM and analytic solutions in steady-state potential problems. Eng Anal Bound Elem 2002;26(7):597–611.
[43] Liu Z, Dong C. Automatic coupling of ABAQUS and a boundary element code for dynamic elastoplastic problems. Eng Anal Bound Elem 2016;65:147–58.
[44] Katsikadelis JT. The boundary element method for engineers and scientists: theory and applications. 2nd ed.. Academic Press; 2016.
[45] Zienkiewicz OC, Taylor RL, Zhu JZ. The finite element method: its basis and fundamentals. Elsevier; 2005.
[46] Liu G-R, Quek SS. The finite element method: a practical course. Butterworth-Heinemann; 2013.
[47] Gong Y, Dong C, Qin F, Hattori G, Trevelyan J. Hybrid nearly singular integration for three-dimensional isogeometric boundary element analysis of coatings and other thin structures. Comput Methods Appl Mech Engrg 2020;367:113099.
[48] Beer G, Smith I, Duenser C. The boundary element method with programming: for engineers and scientists. Springer Science & Business Media; 2008.
[49] Simulia D. Abaqus 6.11 analysis user's manual. In: Abaqus 6.11 documentation. 2011, p. 22.
[50] Gong Y, Trevelyan J, Hattori G, Dong C. Hybrid nearly singular integration for isogeometric boundary element analysis of coatings and other thin 2D structures. Comput Methods Appl Mech Engrg 2019;346:642–73.